Dynamic rupture of crosscutting faults: A possible rupture process for the 2007 Mw 6.6 Niigata-ken Chuetsu-Oki earthquake

Hideo Aochi, Aitaro Kato

Dynamic rupture of cross-cutting faults: A possible rupture process of the 2007 Mw6.6 Niigata-Ken Chuetsu-Oki earthquake

Hideo Aochi
h.aochi@brgm.fr
Natural Risks and CO2 Storage Security Division, BRGM
3 avenue Claude Guillemin, 45060 Orléans Cedex 2 France

Aitaro Kato
akato@eri.u-tokyo.ac.jp
Earthquake Research Institute, the University of Tokyo
1-1-1 Yayoi, Bunkyo-ku, Tokyo, 113-0032, Japan

Abstract

The 2007 Mw6.6 Niigata-Ken Chuetsu-Oki earthquake implies a complex fault mechanism. Several surveys suggest the possibility of two main segments crosscutting each other at the middle, namely north-western dipping in the north and south-eastern dipping in the south. We numerically model dynamic rupture propagation along the inferred segmented fault system using a boundary integral equation method (BIEM). The possibility of the rupture transfer is numerically shown and two rupture modes are reported. Simultaneous rupture transfer along the overlapping part is possible only if stress is highly loaded, however this rupture mode provides a too much slip amount in the result. In the other case where regional stress is relatively low but pore pressure is high enough to govern the rupture criterion (described as low frictional coefficient case in this study), the rupture transfer to the other segment does not occur until the rupture terminates on the first segment regardless of the crosscutting distance between two segments. In this case at the middle cross-cutting part, a possible rupture scenario is that there occur rupturings sequentially in different directions; first on the north-western dipping segment by southbound rupture and on the south-eastern dipping segment by northbound rupture a few seconds later. The simulated rupture scenario on conjugated faults can be strongly led by pre-existing fault structure formed by both the Miocene rifting during an opening stage of the Japan Sea and the subsequent shortening of the crust. Our results infer the importance of investigating earthquake rupture scenarios in complex fault system based on the geophysical and geological information, and the dynamic rupture mechanics.

1. Introduction

How does material rupture under a load? For figuring out the problem clearly, let us think a two-dimensional profile where there are two potential orientations of fault plane, called "conjugate", with respect to the loaded principal force (e.g. Scholz, 2002). Usually all materials break selectively along either dominant plane but they do not rupture on both planes simultaneously. Once one plane becomes dominant in the material, the other plane is no longer activated in terms of stress concentration.

Earthquakes are one of the largest rupture phenomena in a solid material. Fault system has already evolved intensively in the Earth's interior, by interacting and evolving as a geodynamical system over different scales of time and space, so that the characteristics of the materials and the rupture mechanism of earthquakes can be more complex than observed in rock specimens in laboratory experiments. Geologists have pointed out the role played by fault geometry on earthquake rupture (e.g. King and Nabelek, 1985). This can be quantitatively simulated as a dynamic rupture process, as shown in the case of the Mw7.2 1992 Landers, California earthquake by Aochi and Fukuyama (2002), for example. Although this earthquake shows a complex geometry, with bends, branches and segmentations, it can be treated as a single fault plane from the viewpoint of standard seismological description (Olsen et al., 1997).

The Mw6.6 Niigata-ken Chuetsu-Oki earthquake occurred on 16 July 2007 in north-eastern Japan (Figure 1). The hypocenter was located under the Sea of Japan at a depth of around 12 km and several kilometres from the coastline of the main island. The ruptured area expanded

over a length of about 30 km, according to various studies, and part of the rupture may have occurred beneath the main island. Although the focal mechanism clearly showed reverse faulting, it was difficult to determine the fault plane only from the seismological waveform inversion of finite source parameters (Koketsu et al., 2007; Aoi et al., 2008). Extensive seismological and geophysical surveys have been carried out to record the aftershocks for imaging the event distribution and geophysical structure, and to construct the source model. The final results determined by the dense temporal seismic network deployed after the mainshock show a clear variation in aftershock distributions on cross-sections from north to south along the fault strike, as shown in Figure 1 (Kato et al., 2008; Shinohara et al., 2008), with a north-western dip in the north but a south-eastern dip in the south. Furthermore, fine tomography studies elucidate that there is a segment boundary zone situated between the north and the south, which is coincident with the complex aftershock zone where many conjugate fault planes exist (Kato et al., 2008). Although a southeastward-tilted structure of the basement is dominant in the south, a northwestward-tilted structure of the basement gradually develops toward the north (Kato et al., 2008, 2009). It is considered that the lateral complex variations in basement structure along the fault strike have been formed by both the Miocene rifting during the opening stage of the Japan Sea and the subsequent shortening of the crust (e.g., Okamura et al., 1995; Kato et al., 2009). These results indicate that two ruptured segments could be cross-cutting each other in the middle (CT-section in Figure 1). The analyses of geodetic deformation based on InSAR images also support the segmented fault models, mainly because of the irregular pattern of surface deformation from north to south (Aoki et al., 2008; Nishimura et al., 2008, 2009). Recently, Takenaka et al (2009) has demonstrated that the mainshock rupture initiated and propagated on the northwest-dipping plane to the updipward, using the initial rupture phase of the P-wave portion. This

seismological evidence suggests the sequential or simultaneous rupture of the two conjugate fault planes.

From a geological point of view, fault traces can cross each other so as to be consistent with orientations of the regional tectonic stress, although this does not assure that earthquake rupture can occur simultaneously on both fault traces. For example, the 1994 M6.8 Northridge and the 1971 M6.6 San Fernando earthquakes occurred on adjacent thrust faults, which are dipping in opposite directions, i.e. conjugate (Carena and Suppe, 2002). However, there is little evidence of simultaneous activation of two conjugate fault planes. The 1997 Kagoshima, Japan, earthquake (M6.0) shows the possibility of simultaneous rupture on conjugated, adjacent strike-slip segments (Horikawa, 2001). This configuration has been numerically simulated as two separated segments (Kase and Kuge, 2001). In the case of the 2000 Tottori, Japan, earthquake (M6.7), some secondary segments perpendicular to the main traces segments were identified and numerically modelled (Fukuyama et al., 2003; Fukuyama, 2003). However, they remain secondary. Thus the 2007 Niigata-ken Chuetsu-Oki earthquake is a unique occasion to observe simultaneous or sequential rupture on two-conjugated fault planes crosscutting in the middle. This study aims to understand how this is possible from a mechanical viewpoint, through numerical simulations.

2. Numerical Method and Fault Models

We adopt in this study a boundary integral equation method (BIEM) (Aochi et al., 2000) for simulating the dynamic rupture process on complex fault geometry with a given rupture criterion. This method is powerful for various elasto-dynamic problems, especially including discontinuous cracks, which can spontaneously propagate along a given crack geometry, or in

the case of an unknown geometry (e.g. Kame and Yamashita, 1999). As the mainshock hypocenter depth is around 12 km on the north-western dipping fault plane (Figure 1) and most of aftershocks are distributed within the basement in a depth range of 6-15 km where the P-wave velocity is greater than 6 km/s (e.g., Kato et al., 2008; Shinohara et al., 2008), it is sufficient to model this earthquake in an infinite medium without taking into account of the ground surface effect. As the method is strictly based on the theory of infinitesimal deformation in linear elasticity, no numerical nuisance occurs at crack junctions, as successfully shown for crack branching (Tada and Yamashita, 1997; Aochi et al., 2002). In the descretized formulation of the BIEM, stress is always evaluated at the center of each planar discretized element where slip velocity is assumed constant during a time step. We are able to generate the fault geometry model avoiding the kinematic problem of at any jointing points between elements. Such configurations are still difficult to study with other volumetric numerical methods, because a junction point should have some values of displacement, which is not always consistent with the kinematics (e.g. Andrews, 1989).

Figure 2 shows the fault model to be simulated in this study. The northern segment (Segment 1) is 10.4 km long and 8 km wide and the southern segment (Segment 2) is 20 km long and 14.4 km wide. We calibrate these geometries based on Figure 1, namely the relocated aftershock distribution and the hypocenter of the mainshock (Kato et al., 2008). Nevertheless, there remains slight uncertainty especially in the dip angle (δ) of Segment 2 and the crosscutting distance (L) of the two segments. The former is due to a lower resolution for off-shore analysis and the latter is too small to be determined seismologically. The latter is because it is always difficult to determine precisely the fault extension only from the aftershock distribution. Therefore we vary these two parameters in the simulations. The other model parameters are summarized in Table 1. The medium property is consistent with the

tomographic image of velocity near the earthquake source (Kato et al., 2008). The simulation is carried out on a parallel computer, requiring only about 10 minutes for the first 200 time steps using 8 cores.

3. Rupture criterion and stress field

3.1 Slip-weakening law and Coulomb law

The analysis of focal mechanisms of the aftershocks implies that the maximum principal stress axis is on the horizontal plane and perpendicular to the fault strike (Kato et al., unpublished data, 2008; systematical analysis reported on the NIED homepage, http://fnet.bosai.go.jp, 2007). It is consistent with the focal mechanism of the main shock and regional tectonic setting (Kato et al., 2006; Townend and Zoback, 2006). Therefore, we assume that the fault slip direction is purely along the dip, which is also indicated by the focal mechanism of the main shock (Figure 1). On the other hand, this indicates that the main shock releases a part of the accumulated regional stress and does not rotate the stress field. The rupture process is governed by a constitutive relation between on-going fault discontinuity Δu and shear stress τ called as slip-weakening law, which is widely accepted in dynamic rupture process of earthquakes (e.g. Ida, 1972, Palmer and Rice, 1973). We adopt the following standard mathematical expression:

$$\left|\tau(\Delta u)\right| = \tau_r + (\tau_p - \tau_r)(1 - \left|\Delta u\right| / D_c) H(1 - \left|\Delta u\right| / D_c) \quad (1)$$

where $H(\cdots)$ is a Heaviside function, τ_p and τ_r are peak and residual stresses and D_c is critical slip-weakening displacement, also shown in Figure 3. Here we explicitly write down Equation (1) with absolute values, because loaded shear stress on two segments has mechanically opposite sign so that slip direction is reversed in a mechanical view. This corresponds to the seismological description where fault strike is in reverse although fault rake is the same. Before the onset of dynamic rupture, namely in the case of $|\Delta u| = 0$, shear stress $|\tau|$ remains lower than τ_p. τ_p and τ_r are given by the Coulomb law, namely a product of the frictional coefficient (μ_s: static or μ_d: dynamic frictional coefficients) and applied normal stress σ_n as:

$$\tau_p = \mu_s \times \sigma_n, \text{ and} \qquad (2)$$

$$\tau_r = \mu_d \times \sigma_n \quad . \qquad (3)$$

In the following simulations, fault strength and applied stress is determined uniquely by the assumed tectonic regional stress assuming a single value of μ_s in a simulation without privileging any direction of fault geometry. As τ_p and τ_r change significantly according to the assumption, we give the same slip-weakening rate ($\equiv (\tau_p - \tau_r) / D_c$) for all the cases instead of fixing a value of D_c, namely = 30 [MPa/m], which is consistent with the value inferred from the seismological analyses (e.g. Ide and Takeo, 1997; Olsen et al., 1997). This also allows us to initiate the dynamic rupture in the same way, as the rupture propagation criteria is controlled by the slip-weakening rate (Matsu'ura et al., 1992; Madariaga and Olsen, 2000). We give Segment 1 an initial circular crack of a radius of 1 km where the strength is

supposed to drop instantaneously at the beginning of the simulation in order to initiate the spontaneous dynamic rupture propagation.

3.2 Tri-axial compression stress field

We assume a uniform compressional tectonic stress around the source area. The maximum principal stress is taken to be horizontal, perpendicular to the fault strike, and the minimum one is vertical, namely pressure by gravity. The intermediate one should be horizontal, parallel to the fault strike, but as we suppose a pure reverse faulting, this component does not play a role in the dynamic modelling. The initial shear and normal stresses applied on the fault segments are given respectively by:

$$\tau_0 = \frac{\sigma_1 - \sigma_3}{2} \sin 2\Phi \text{, and} \qquad (4)$$

$$\sigma_n^{\,0} = \frac{\sigma_1 + \sigma_3}{2} - \frac{\sigma_1 - \sigma_3}{2} \cos 2\Phi, \qquad (5)$$

letting σ_1 and σ_3 be the maximum and minimum principal stresses (compression taken as positive), and Φ be the angle of the fault segment inclined with respect to the σ_1 axis. The model parameters are summarized in Table 1. In the mechanical coordinate we take, Equation (4) gives a positive shear stress loading on Segment 1, while it gives a negative loading on Segment 2. This means that, in the same coordinate, fault slip is positive on Segment 1 but negative on Segment 2. Hereafter the simulations results are presented based on this sign convention.

What is known is the minimum principal stress σ_3 in the vertical direction. We take the hydrostatic condition at a depth of z = 8 km where cross-cutting section is located. We precise that all the normal stresses are effective normal stresses, since the effect of pore pressure is subtracted. Therefore,

$$\sigma_3 = P(z = 8km) = (\rho - \rho_H) gz = 117.6 \text{ MPa}, \quad (6)$$

where ρ is the material density (Table 1), ρ_H is the water density and g is the gravity constant. We suppose $\mu_s = 0.7$ as inferred from the laboratory experiments (e.g. Byerlee, 1978) and illustrate the Mohr circle so as not to exceed the rupture criterion imposed by the frictional line defined by $\mu_s = 0.7$ (Figure 4(a)). The angle most favourable to the rupture is $\Phi = 27.5°$ from simple algebra. In this case as summarized in Table 2, we obtain $\sigma_1 = 433.9$ MPa and a strength excess on Segment 1 of 56.5 MPa. In Figure 4, for reference, we add dynamic friction (residual stress) lines of $\mu_d = 0.33$ which gives the S value of 1 on Segment 1, defined by

$$S = \frac{\tau_p - |\tau_0|}{|\tau_0| - \tau_r}, \quad (7)$$

(Das and Aki, 1977), namely strength excess is equal to static stress drop (at the initial normal stress). This condition is quite natural for allowing the dynamic rupture on a plane fault in the term of the value S (S ≈ 1), but it should be noted that μ_d is half of μ_s. In other words, about half of the absolute stress is relieved due to the earthquake rupture and its amount is an order of 50 MPa, which seems to be still high comparing to the averaged value inferred from the

natural earthquakes. If we taken a higher value of μ_d, for example, $\mu_d = 0.7\mu_s$, S value is 7.9 for Segment 1, which does not allow the initiation of rupture in our situation.

The fault strength may be much weaker for example due to over-pressure of existing fluid (e.g. Miller et al., 2004; Sibson, 2007). Actually the fluid existence is inferred at the lower crust beneath the fault system from the tomographic interpretation (Kato et al., 2009). Although we do not aim to discuss the detail of such complex mechanism, we instead present it by lower frictional coefficients. Figure 4(b) shows the stress configuration assuming $\mu_s = 0.3$. The most favourite angle of fault plane is $\Phi = 36.7°$. In this case, we get $\sigma_1 = 212$ MPa and $\mu_d = 0.24 \approx 0.6\ \mu_s$ for the condition of S = 1 on Segment 1.

It is worth of discussing different parameter settings in a fault system of complex geometry as the effect of fluid overpressure is not yet quantified in the earthquake rupture. We test three cases, $\mu_s = 0.7$, 0.5 and 0.3. As explained above (e.g. Figure 4) and summarized in Table 2, a higher value of the frictional coefficient corresponds to a high stress condition (strong fault strength), while a lower value implies a lower stress (strength) condition with significant pore fluid effect. We have not introduced here any depth-dependence on the model parameters. However the fault system is located at depth enough in the seismogenic zone so as not to be suffered from the significant depth-dependency in the shallow or subsurface crustal structures. We recall that the main objective of this paper is to investigate the mechanics of rupture transfer from one segment to another along the intersection which is located at the same seismogenic depth from north to south. This is why our parameter choice does not lose the generality of mechanics.

4. Simulation results

Is it possible that the crosscutting conjugate faults rupture simultaneously? If so, how does it occur? For investigating the possible mechanism, we make three parameters variable as explained in the previous sections, namely the dip (δ) of Segment 2, the overlapping length (L) of two segments and the static frictional coefficient (μ_s) . We carry out 45 simulations in total. Figure 5 shows snapshots of two typical dynamic rupture scenarios found among the numerical simulations, and Figure 6 summarises the scenarios by parameters.

The first example (case $\mu_s = 0.7$, $\delta = 35°$ and $L = 4$ km) shows that rupture transfer on Segment 2 occurs simultaneously during the rupture propagation on Segment 1 (Figure 5a). The triggering is usually caused by strong perturbation of dynamic stress field brought from Segment 1, and this scenario is due to the very low value of parameter S on Segment 2 (close to 0) as inferred from Figure 4. We found that the initial condition is much more favour on Segment 2 than Segment 1. This occurs commonly for the fault geometry of Segment 2 with a dip angle δ of 30-40° indifferently from the frictional parameter μ_s and the crosscutting distance L (except for $L = 0$). The rupture initiates on Segment 2 immediately when a favourite stress wave (dynamically there are more or less both positive and negative changes) arrives and begin to propagate spontaneously. This kind of scenario is often found in our simulations of this study. This is due to the extreme condition naturally generated for the conjugate faults under a uniform stress field. In the case of parallel faults, for example, applied stress is the same for both so that it is difficult to favour Segment 2 (e.g. Harris and Day, 1999; Kase and Kuge, 2001). In the branched fault cases, it is reported that rupture can transfer to the secondary plane other than the principal plane where the rupture starts (Aochi

et al., 2002; Kame et al., 2003), however rupture mode is continuously the same in these cases (slip direction with respect to the fault direction). The particularity of our study is that slip direction is different on two segments, although they are both reverse faulting with respect to the geological description.

Another example (case $\mu_s = 0.3$, $\delta = 45°$ and $L = 4$ km) of Figure 5(b) presents sequential rupture propagation from Segment 1 to Segment 2. It is natural that this occurs when two segments are not overlapping each other in Figure 6 ($L = 0$). More generally, this is observed when frictional coefficient μ_s (namely stress) is lower (see again Figure 6), namely when stress concentration is required more to initiate rupture process on Segment 2. In this case, we emphasis on the fact that rupture on Segment 2 is not initiated during the rupture propagating along Segment 1 so that the rupture transfer is independent of the overlapping length of the segments. Figure 7 confirms the process in detail for the observed cases, showing the rupture time propagation on Segment 2. Segment 2 is not activated during the rupture propagation on Segment 1. It is called as shadow effect, or simply stress concentration is the most beyond the rupture front on the same plane. The rupture on Segment 2 begins from the point where the Segment 1 stops. It is then observed that the rupture on Segment 2 continues propagating to the south, while a part of the rupture comes back in the north direction on Segment 2 so as to fill the overlapping portion. In these cases, at the middle of this fault system where two faults planes are cross-cutting, two fault planes are ruptured with a time lag of a few seconds during a single earthquake. Namely, the north-western dipping rupture may have taken place first towards the south, and then the south-eastern dipping rupture starts later and propagates to both the north and the south.

There is another scenario that rupture does not transfer on Segment 2 (Figure 5c). This is found when $\delta = 50°$, the same dip as Segment 1, namely frictional and initial stress conditions are the same on both segments. As a result, it is in any case required that Segment 2 has a more favourable condition than Segment 1 in order for rupture to transfer.

5. Discussion

In the previous section, we have focused on the mechanical scenario of rupture transfer between conjugate segments. It is still difficult to argument which parameter setting adapts better with the 2007 Niigata-ken Chuetsu-Oki earthquake. Concerning about frictional coefficient μ_s, any value allows rupture transfer on Segment 2. However it leads quantitatively different slip amount according to the allowed stress drop. In this meaning, a high μ_s gives a too much slip more than 10 m with respect to the fault dimension. Note that rupture never begins at the hypocenter when a relatively high μ_d is given (large S value). Therefore a low value of μ_s adjust better the amount of slip expected for such fault dimension. About the fault geometry of Segment 2, a low dipping angle around 30° is inferred from the aftershock distribution (Kato et al., 2008; Shinohara et al., 2008), but they also note that this dip angle δ may be more steep because of the incertitude of their hypocenter localization off shore. This is why we have varied this parameter. As long as the friction coefficient μ_s is high, this angle δ does not play a significant role as stress is loaded too much on Segment 2 of a wide range of dip angle δ. For a smaller value of μ_s, the possibility of rupture transfer does not change (a wide angle of δ between 30-45°). This is acceptable with respect to the incertitude of the observations. By the way, we do not have any direct indication on the crosscutting distance *L*, although the aftershock distribution (Figure 1) supports the cross-

cutting two segments at the middle. Our simulation shows the possibility of simultaneous rupture transfer for a high frictional coefficient, while rupture transfers sequentially one from one in other cases, for which it is essential that Segment 1 is terminated. Interpretation from the structural geology implies rather such discontinuity in fault geometry between the north and the south (Kato et al., 2008; 2009).

In this study, we have assumed a simple, but extreme Mohr–Coulomb criterion, in which the static friction line is tangential to the Mohr circle. Namely the applied stress reaches the rupture criterion at a direction (Φ) and some tested geometries are very close to this point (see Figure 4 and S values listed in Table 2). It is then naturally expected that rupture transfer between segments is very easy. It is possible to consider that Segment 1 is not optimally oriented for failure but is weaker than the surrounding rocks or that Segments 1 and 2 are governed by different failure conditions. However it is too difficult to quantify such difference in any general way. By the way, when the Mohr circle is smaller (stress is less loaded), the rupture transfer possibility is more limited for the fault geometry around the angle defined by Φ and a sequential rupture transfer becomes more dominant. Therefore the rupture transfer on Segment 2 does not begin before the rupture termination on Segment 1, as often reported for rupture triggering between segmented faults (e.g. Kase and Kuge, 2001). This evidence also supports the termination of Segment 1 to the south.

In the mechanical meaning it may be interesting to study the case where two segments are separated with a spatial gap. However from the aftershock distribution and the inferred finite source model, it is natural to think that two faults are overlapping or connecting each other for the 2007 Niigata-ken Chuetsu-Oki earthquake. In any case, two separated faults have been already studied by many authors since 1990's (e.g. Harris and Day, 1999; Kase and Kuge,

2001). The distance allowing fault jump is often considered a few kilometres, but Kase et al. (2009) allow a rupture jump over a jog of 10 km distance for the 1668 North Anatolian earthquake. It is true that the existence of a gap between segments makes it difficult for the rupture to transfer, but one has to keep in mind that this quantitative possibility strongly depends on the given stress and frictional condition.

It is still difficult to compare the detailed processes found in our simulations with the seismological observations, as different finite source models fit both near-field and teleseismic data (e.g. Koketsu et al., 2007; Aoi et al., 2008). It is reported that conjugate faults gives a better fit of the observed seismograms than either one fault model from the view of statistical analysis using Akaike-Baysian Information Criterion (Horikawa, 2008), but this does not mean that any characteristic waveform radiated from conjugate faults is identified. In any cases, the existence of two or three asperities is inferred from north to south along the fault strike. Each kinematic asperity may briefly correspond to the dynamic rupture of each segment in our simulations. Comparing our results to those from geodetic inversion (Nishimura et al., 2008, 2009), the inverted fault slip is concentrated on the area of our fault model. We cannot currently answer why the 2007 earthquake did not begin on Segment 2 but on Segment 1. In our simulation, Segment 1 is not always more favourable than Segment 2 in terms of initial stress and the Mohr-Coulomb criterion (e.g. Figure 4). It is an unsolved problem whether the rupture starting point (hypocenter) of large earthquakes is selected deterministically or randomly (Ide and Aochi, 2005). On the particular occasion of the Niigata region, it is suggested that strengths of highly-dipping faults like the Segment 1 may be slightly weaker than those of low-dipping faults like the Segment 2, due to a high-fluid pressures beneath the seismogenic zone and within the fault zones (Sibson, 2007). Spatial

distribution of fluid pressure within the crust could be a key factor controlling initiation points of earthquake ruptures for this region.

The potential of rupture propagation across the cross-cutting conjugate faults shown by the present study is significant to seismic hazard analysis. The active fault traces are frequently used for the estimation of rupture lengths and potential magnitudes. Since the fault traces are usually not continuous and are composed of several segments separated by fault steps, the dimension of a fault step is a good indicator for the continuity of the earthquake rupture, and plays an important role in estimating potential magnitudes. A limiting dimension of fault step above which earthquake ruptures terminate is reported to range from 3 to 4 km for the case of strike-slip faults, empirically from the surface trace observations (Wesnousky, 2006). However, about the cross-cutting conjugate thrust-faulting at seismogenic depths, even if the fault surface traces are separated by distances greater than several ten-kilometres, there remains a potential for the earthquake rupture to propagate across the cross-cutting conjugate faults as illustrated in the present study. The rupture transfer across the cross-cutting conjugate faults as like this example ends by a longer rupture length and a bigger magnitude than the estimation simply based on each fault surface trace (no interaction is considered between conjugate faults for any seismic hazard evaluation). It has been observed that cross-cutting conjugate faults are well developed in fold and thrust zones, where thick sedimentary layers are piled up, such as the Coalinga region in California (e.g., Eberhart-Philips, 1989) and the EI Asnam fault zone in Algeria (Chiarabba et al., 1997). Thus, imaging of deep geometries of active faults beneath the thick sediments is essentially important to evaluate potential magnitudes within active fold and thrust zones.

6. Summary

In this study we are able to simulate the dynamic rupture propagation process in a crosscutting conjugate fault system as one proposed scenario of the 2007 Niigata-ken Chuetsu-Oki earthquake. The rupture transfer possibility is very sensitive for the given frictional and stress condition. However for a dip of around 30-45° of Segment 2, its possibility is numerically shown for any frictional levels and independently of the crosscutting distance. Two types of rupture mode are found. If stress is loaded highly under the hydrostatic condition, a simultaneous rupture on both segments is possible along the overlapping part and the triggered rupture on Segment 2 becomes dominant. In other cases where regional stress is not so high but pore pressure plays a significant role to govern the rupture criterion (low frictional coefficient case in this study), rupture does not transfer on Segment 2 until it terminates on Segment 1 regardless of the crosscutting distance. From the view point of the resultant slip amount expected for this dimension of fault planes, a low frictional condition under the high pore pressure existence is strongly preferred. The 2007 Niigata-ken Chuetsu-Oki earthquake offers an important insight into potential scenario of earthquake rupturing, i.e. that they are dynamically governed by the existing fault structure associated with Miocene rifting during an opening stage of the Japan Sea and the subsequent shortening of the crust. The numerical work undertaken in this study should allows us to understand better the mechanics of the dynamic rupture of earthquakes, the importance of structural geology and, consequently, the details of the rupture process.

Acknowledgments

We thank the group that undertook aftershock observations of the 2007 Niigata-ken Chuetsu-Oki earthquake for their data, which encouraged our work. The comments and suggestions from two anonymous reviewers and the associate editor are very useful for improving our models and discussion. H. A thanks the international office of the Earthquake Research Institute, the University of Tokyo for his invited stay in 2007 when this work began. This is also a contribution to the French national projects funded by ANR Catastrophes Telluriques et Tsunamis 2005 and Risques Naturels 2008.

References

[1] Andrews, D. J. (1989), Mechanics of fault junctions, *J. Geophys. Res.*, 94, 9389-9397.

[2] Aochi, H. and E. Fukuyama (2002), Three-dimensional nonplanar simulation of the 1992 Landers earthquake, *J. Geophys. Res.*, 107, doi:10.1029/2000JB000061.

[3] Aochi, H., E. Fukuyama, E. and M. Matsu'ura (2000), Spontaneous rupture propagation on a non-planar fault in 3D elastic medium, *Pure appl. Geophys.*, 157, 2003-2027.

[4] Aochi H., R. Madariaga and E. Fukuyama (2002), E. Effect of normal stress during rupture propagation along nonplanar faults, *J. Geophys. Res.*, 107, doi:10.1029/2001JB000500.

[5] Aoki, T., M. Furuya, and T. Kato (2008), Coseismic deformation due to the 2007 Chuetsu-oki earthquake (Mw = 6.8), *Earth Planets Space*, 60, 1075-1080.

[6] Aoi, S., H. Sekiguchi, N. Morikawa and T. Kunugi (2008), Source process of the 2007 Niigata-ken Chuestu-oki earthquake derived from near-fault strong motion data, *Earth Planets Space*, 60, 1131-1135.

[7] Byerlee, J. D. (1978), Friction of rocks, Tectonophysics, 9, 475-486.

[8] Carena, S. and Suppe, J. (2002), Three-dimensional imaging of active structures using earthquake aftershocks: the Northridge thrust, California, *J. Struc. Geol.,* 24, 887-904.

[9] Chiarabba, C., A. Amato, and M. Meghraoui (1997), Tomographic images of the EI Asnam fault zone and the evolution of a seismogenic thrust-related fold, *J. Geophys. Res.*, 102, 24485-24498.

[10] Das, S. and K. Aki (1977), A numerical study of two-dimensional spontaneous rupture propagation, *Geophys. J. R. Astron. Soc.* 50, 643-668.

[11] Eberhart-Philips, D. (1989), Active Faulting and Deformation of the Coalinga Anticline as Interpreted From Three-Dimensional Velocity Structure and Seismicity, *J. Geophys. Res.*, 94, 15565-15586.

[12] Fukuyama, E. (2003), Earthquake dynamic rupture and stress field around the fault, *J. Geography*, 112, 850-856.

[13] Fukuyama, E., W. L. Ellsworth, F. Waldhauser, and A. Kubo (2003), Detailed fault structure of the 2000 western Tottori, Japan, earthquake sequence, *Bull. Seism. Soc. Am.*, 93, 1468-1478.

[14] Harris, R. A. and S. M. Day (1999), Dynamics of fault interaction – parallel strike-slip faults, *Geophys. Res. Lett.*, 26, 2089-2092.

[15] Horikawa, H. (2008), Source model of the 2007 Chuestsu-Oki earthquake, technical note in Active Fault Research Center News, 75, 1-3.

[16] Horikawa, H. (2001), Earthquake doublet in Kagoshima, Japan: Rupture of asperities in a stress shadow, *Bull. Seism. Soc. Am.*, 91, 112-127.

[17] Ida, Y. (1972), Cohesive force across the tip of a longitudinal-shear crack and Griffith's specific surface energy, *J. Geophys. Res.*, 77, 3796-3805.

[18] Ide, S. and H. Aochi (2005), Earthquakes as multiscale dynamic ruptures with heterogeneous fracture surface energy, *J. Geophys. Res.*, 110, B11303, doi:10.1029/2004JB003591.

[19] Ide, S. and M. Takeo (1997), Determination of constitutive relations of fault slip based on seismic wave analysis, J; Geophys. Res., 102, 27379-27391.

[20] Kame, N., J. R. Rice and R. Dmowska (2003), Effect of pre-stress state and rupture velocity on dynamic fault branching, *J. Geophys. Res.*, 108, doi:1029/2002JB002189.

[21] Kame, N. and T. Yamashita (1999), Simulation of the spontaneous growth of a dynamic crack without constraints on the crack tip path, *Geophys. J. Int.,* 139, 345-358.

[22] Kase, Y. and K. Kuge (2001), Rupture propagation beyond fault discontinuities: significance of fault strike and location, *Geophys. J. Int.*, 147, 330-342.

[23] Kase, Y., H. Kondo and Ö. Emre (2009), Dynamic rupture process of the great 1668 North Anatolian earthquake, *in the proceedings of the French-Japanese workshop on earthquake source*, October 2009, Paris-Orléans, France.

[24] Kato, A., S. Sakai, N. Hirata, E. Kurashimo, T. Iidaka, T. Iwasaki, and T. Kanazawa (2006), Imaging the seismic structure and stress field in the source region of the 2004 mid-Niigata Prefecture earthquake: Structural zones of weakness and seismogenic stress concentration by ductile flow, J. Geophys. Res., 111, B08308, doi:10.1029/ 2005JB004016.

[25] Kato, A., S. Sakai, E. Kurashimo, T. Igarashi, T. Iidaka, N. Hirata, T. Iwasaki, T. Kanazawa, and Group for the aftershock observations of the 2007 Niigataken Chuetsu-oki Earthquake (2008), Imaging heterogeneous velocity structures and

complex aftershock distributions in the source region of the 2007 Niigataken Chuetsu-oki Earthquake by a dense seismic observation, *Earth Planets Space*, 60, 1111-1116.

[26] Kato, A., E. Kurashimo, T. Igarashi, S. Sakai, T. Iidaka, M. Shinohara, T. Kanazawa, T. Yamada, N. Hirata, and T. Iwasaki (2009), Reactivation of ancient rift systems triggers devastating intraplate earthquakes, *Geophys. Res. Lett.*, 36, L05301, doi:10.1029/2008GL036450.

[27] King, G. and J. Nabelek (1985), Role of fault bends in the initiation and termination of earthquake rupture, *Science*, 228, 984-987.

[28] Koketsu, K., H. Miyake and K. Hikima (2007), Source Inversion for the 2007 Chuetsu-oki, Japan, Earthquake: A Case of Difficulty Determining the Source Fault Plane, *Eos Trans.* AGU, 88(52), Fall Meet. Suppl., Abstract, S54A-05.

[29] Madariaga, R. and K. B. Olsen (2000), Criticality of rupture dynamics in 3-D, *Pure Appl. Geophys.*, 157, 1981-2001.

[30] Matsu'ura, M., H. Kataoka and B. Shibazali (1992), Slip-dependent friction law and nucleation processes in earthquake rupture, *Tectonophysics*, 211, 135-148.

[31] Miller, S. A., C. Collettini, L. Chiaraluce, M. Cocco, M. Barchi, and B. Kaus (2004), Aftershocks driven by a high pressure CO2 source at depth, Nature, 427, 724-727.

[32] Nishimura, T., M. Tobita and M. Murakami (2008), Fault model of 2007 M=6.8 Chuetsu-oki earthquake, Central Japan, constructed using geodetic data, *Earth Planets Space*, 60, 1093-1098.

[33] Nishimura, T., M. Tobita, M. Murakami, T. Kanazawa, and M. Shinohara. (2009): Fault Model of 2007 M = 6.8 Chuetsu-oki earthquake, central Japan, constructed using geodetic data, *Advances in Geosciences* (Proceedings of Asia Oceania Geosciences Society 2008), in press.

[34] Okamura, Y., M. Watanabe, R. Morijiri, and M. Satoh (1995), Rifting and basin inversion in the eastern margin of the Japan Sea, *The Island Arc*, 4, 166–81.

[35] Olsen, K. B., R. Madariaga and R. J. Archuleta (1997), Three-dimensional Dynamic simulation of the 1992 Landers earthquake, *Science*, 278, 834-837.

[36] Palmer, A. C. and J. R. Rice (1973), The growth of slip surface in the progressive failure of over-consolidated clay, Proc. R. Soc. London, Ser. A., 332, 527-548.

[37] Scholz C. H. (2002), *The Mechanics of Earthquakes and Faulting*, Cambridge University Press, New York.

[38] Shinohara, M., Kanazawa, T., Yamada, T., Nakahigashi, K., Sakai, S., Hino, R., Murai, Y., Yamazaki, A., Obana, K., Ito, Y., Iwakiri, K., Miura, R., Machida, Y., Mochizuki, K., Uehira, K., Tahara, M., Kuwano, A., Amamiya, S., Kodaira, S., Takanami, T., Kaneda, Y., and Iwasaki, T. (2008), Precise aftershock distribution of the 2007 Chuetsu-oki Earthquake obtained by using an ocean bottom seismometer network, *Earth Planets Space*, 60, 1121-1126.

[39] Sibson, R. H (2007), An episode of fault-valve behaviour during compressional inversion? — The 2004 MJ6.8 Mid-Niigata Prefecture, Japan, earthquake sequence, *Earth Planet. Sci. Lett.*, 257, 188-199.

[40] Tada, T. and Yamashita, T. (1997), Non-hypersingular boundary integral equations for two-dimensional non-planar crack analysis, *Geophys. J. Int.,* 130, 269-282.

[41] Takenaka, H., Y. Yamamoto, H. Yamasaki (2009), Rupture process at the beginning of the 2007 Chuetsu-oki, Niigata, Japan, earthquake, *Earth Planet. Space*, 61, 279-283.

[42] Terakawa, T. A. Zoporowski, B. Galvan, and S. A. Miller, Identificatin of the high pressure fluid source driving the L'Aquila earthquake sequence, EOS, U12A-06, 2009.

[43] Townend, J., and M. D. Zoback (2006), Stress, strain, and mountain building in central Japan, J. Geophys. Res., 111, B03411, doi:10.1029/2005JB003759.

Wesnousky, G. S. (2006), Predicting the endpoints of earthquake ruptures, *Nature*, 444, 358-360, doi:10.1038.

1 Table 1: Model parameters used in this study. Variables are shown in *italic*.

2

Model parameters	**Quantity [unit]**
P- *and S*- wave velocities	6000, 3464 [m/s]
Medium density	2500 [kg/m^3]
BIEM element size	300 [m]
BIEM time step	0.025 [s]
Segment 1: Dimension (strike, dip, rake)	10.4 x 8 [km^2] (215°, 50°, 90°)
Segment 2: Dimension (strike, dip δ, rake)	20 x 14.4 [km^2] (35°, *30,35,40,45,50*°, 90°)
Crosscutting distance L	*0, 4, 8* [km]

3

4

5

6

Table 2: Initial conditions and frictional parameters assumed in the simulation. The condition for Segment 2 is shown for a dip of 30°, 40° and 50°, for references. σ_3 is the minimum principal stress (vertical direction) extracting the hydrostatic pore pressure (Equation (6)).

Parameters	Values (in case of stress, unit in MPa)		
Static frictional coefficient μ_s	0.7	0.5	0.3
Effective vertical stress σ_3 ≡ hydrostatic at 8 km depth	117.6	117.6	117.6
Maximum principal stress σ_1	433.8	307.9	212.4
Initial shear stress on Segment 1	155.7	93.7	46.7
Initial normal stress on Segment 1	303.2	229.3	173.3
Required strength excess on Segment 1	56.5	20.94	5.28
S value	1	1	1
Dynamic frictional coefficient μ_d	0.33	0.32	0.24
Initial shear stress on Segment 2	-136.9/-155.7/-155.7	-82.4/-93.7/-93.7	-41.1/-46.7/-46.7

(δ=30°/40°/50°)			
Initial normal stress on Segment 2 (δ=30°/40°/50°)	196.7/248.3/303.2	165.2/196.2/229.3	141.3/156.8/173.3
S value on Segment 2 (δ=30°/40°/50°)	0.01/0.24/1	0.006/0.14/1	0.18/0.037/1

1

Figure captions

Figure 1: The 2007 Niigata-ken Chuetsu-Oki, Japan, earthquake. Relocated aftershock distributions along cross sections and the inferred faulting model as shown by gray-thick lines with arrows denoting slip directions (after Kato et al., 2008). Aftershocks are colored to the depths. The Moment tensor for the mainshock (the NIED) clearly shows reverse faulting but the aftershock distributions demonstrate north-west dipping fault in the north and south-east dipping fault in the south. The direction of the maximum principal stress axis σ_1 is drawn as thick-white arrows.

Figure 2: Fault geometry with respect to the aftershock distribution in three-dimensional space from different angles of view (cross section view in the left panel, and 3D view from southern-east-upper direction in the right panel).The variables in the simulations are the dip angle (δ) of Segment 2 (SE dipping in the south) and the overlapping length (L) between two segments. The mainshock hypocenter is located on the deep part of the Segment 1.

Figure3: Slip-weakening law defined by Equation (1).

Figure 4: Coulomb rupture criterion and Mohr circle in the case of μ_s (a) 0.7 and (b) 0.3. In both cases, the hydrostatic condition at 8 km depth is supposed, namely σ_3 = 117.6 MPa. The dynamic stress level μ_d is drawn so as to S value to be 1 on Segment 1 (see the amount signed by the arrows comparing to Figure 3). The initial condition on Segment 1 is represented by a solid circle and the initial conditions on Segment 2 are shown by triangles for a dip of 30, 40 and 50°.

Figure 5: Snapshots of rupture propagation. For each simulation, slip velocity, fault slip, shear stress change and normal stress change are illustrated at different simulation time. The bold lines show the cross section with the other segment. The arrows show the fault strike in horizontal axis and dip in vertical axes. (a) Simultaneous rupture transfer on Segment 2. (b) Sequential rupture transfer from Segment 1 to 2. (c) Case of no rupture transfer.

Figure 6: Diagram of rupture mode obtained through numerical simulations. (a) $\mu_s = 0.7$, (b) $\mu_s = 0.5$ and (c) $\mu_s = 0.3$, respectively. The double circles represent simultaneous rupture on both segments as shown in Figure 5(a). The single circles means sequential rupture transfer from Segment 1 to Segment 2 such as Figure 5(b). The crosses are the cases that rupture does not transfer on Segment 2.

Figure 7: Rupture time on Segment 2 when $\mu_s = 0.3$ and $\delta = 45°$ for variable over-lapping lenghs *L*. Rupture time at each point on Segment 2 is shown between 3 and 8 seconds after the origin time. The red bold line or point show the position where Segment 1 is cross-cutting.

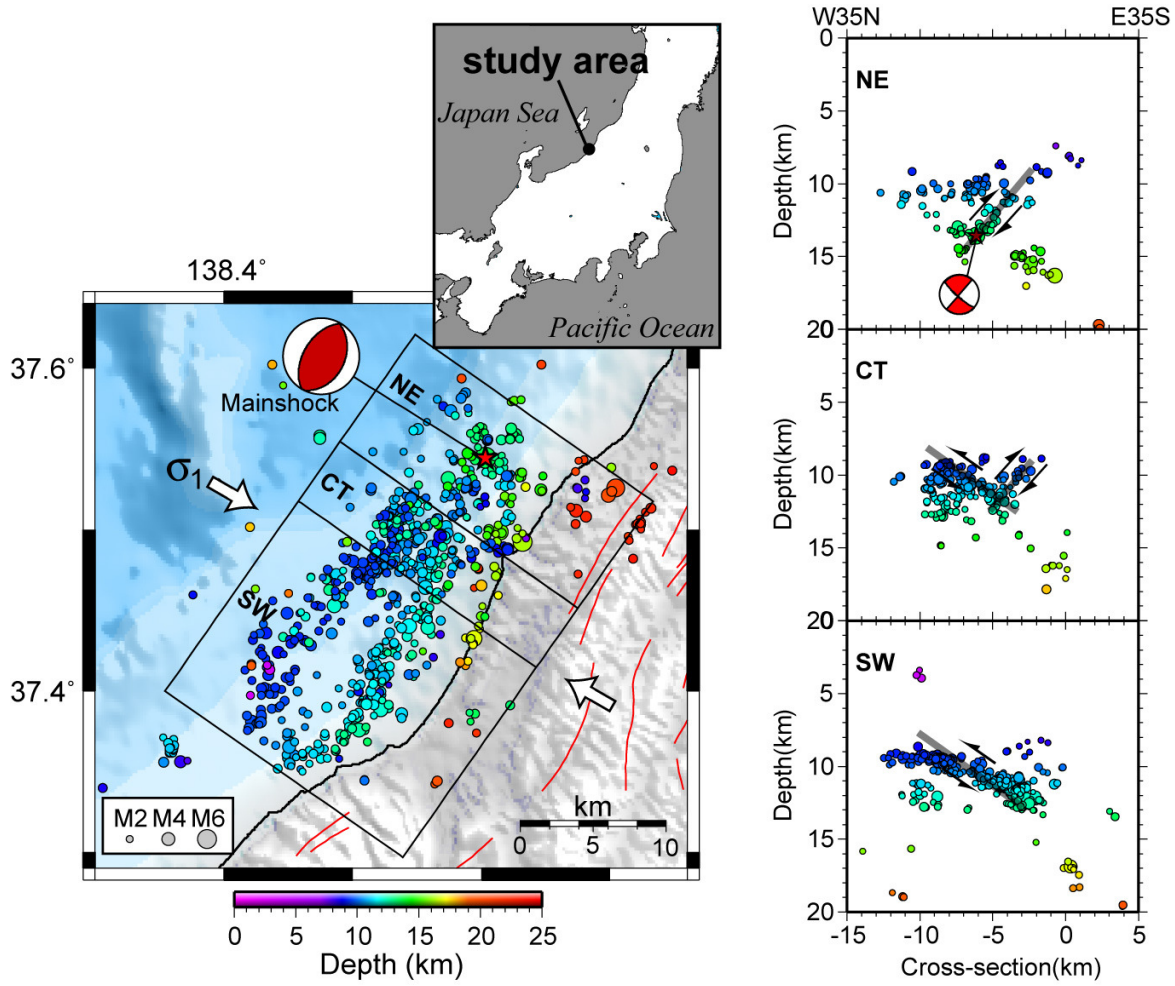
study area
Japan Sea
Pacific Ocean
138.4°
37.6°
37.4°
Mainshock
NE
CT
SW
σ1
M2 M4 M6
km
0 5 10
0 5 10 15 20 25
Depth (km)
W35N
E35S
NE
CT
SW
Depth(km)
-15 -10 -5 0 5
Cross-section(km)

Figure 1.

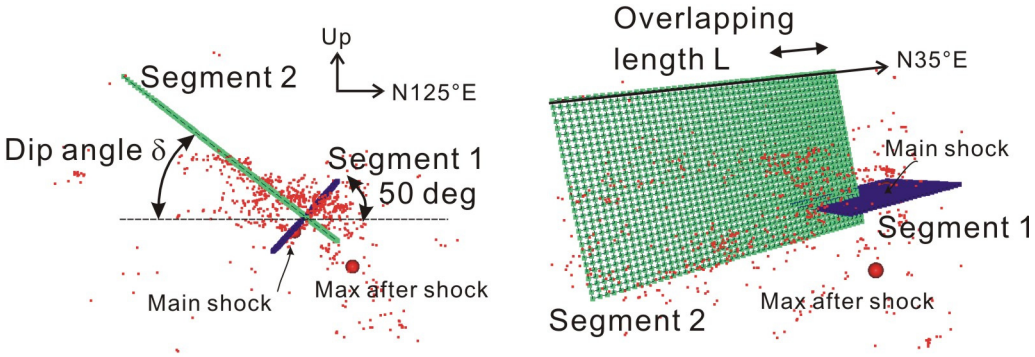
Up
Segment 2
N125°E
Dip angle δ
Segment 1
50 deg
Main shock
Max after shock
Overlapping
length L
N35°E
Main shock
Segment 1
Max after shock
Segment 2

1

2 Figure 2.

3

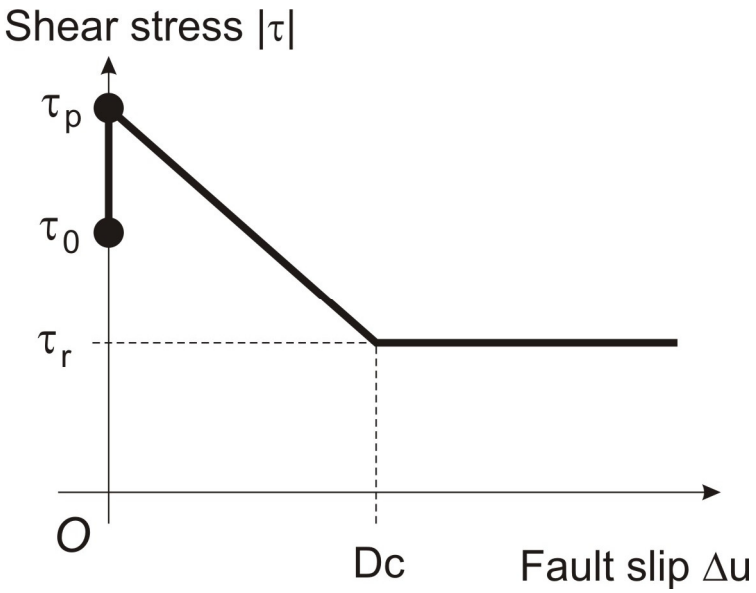

Figure 3.

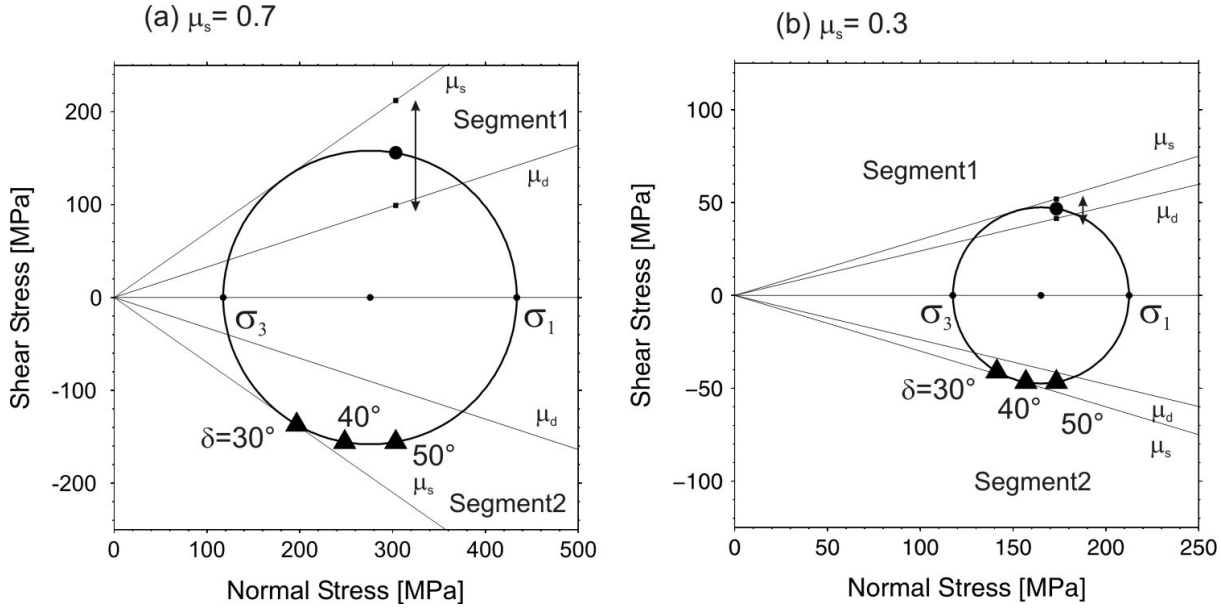
(a) μs= 0.7
Shear Stress [MPa]
Normal Stress [MPa]
μs
Segment1
μd
σ3
σ1
δ=30°
40°
50°
μd
μs
Segment2
(b) μs= 0.3
Shear Stress [MPa]
Normal Stress [MPa]
Segment1
μs
μd
σ3
σ1
δ=30°
40°
50°
μd
μs
Segment2

Figure 4 :

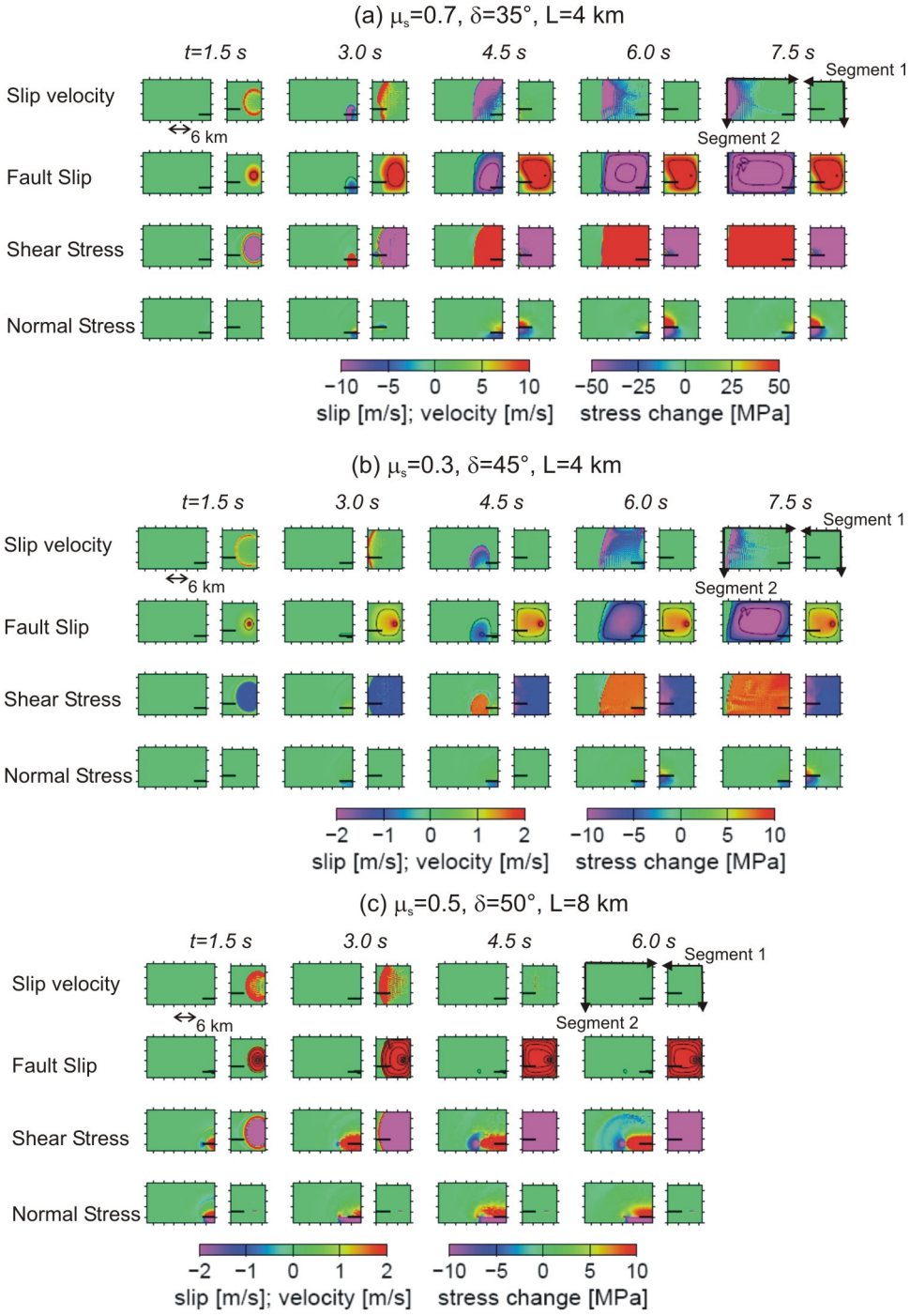
(a) μs=0.7, δ=35°, L=4 km
t=1.5 s
3.0 s
4.5 s
6.0 s
7.5 s
Segment 1
Segment 2
Slip velocity
6 km
Fault Slip
Shear Stress
Normal Stress
−10 −5 0 5 10
slip [m/s]; velocity [m/s]
−50 −25 0 25 50
stress change [MPa]
(b) μs=0.3, δ=45°, L=4 km
t=1.5 s
3.0 s
4.5 s
6.0 s
7.5 s
Segment 1
Segment 2
Slip velocity
6 km
Fault Slip
Shear Stress
Normal Stress
−2 −1 0 1 2
slip [m/s]; velocity [m/s]
−10 −5 0 5 10
stress change [MPa]
(c) μs=0.5, δ=50°, L=8 km
t=1.5 s
3.0 s
4.5 s
6.0 s
Segment 1
Segment 2
Slip velocity
6 km
Fault Slip
Shear Stress
Normal Stress
−2 −1 0 1 2
slip [m/s]; velocity [m/s]
−10 −5 0 5 10
stress change [MPa]

Figure 5.

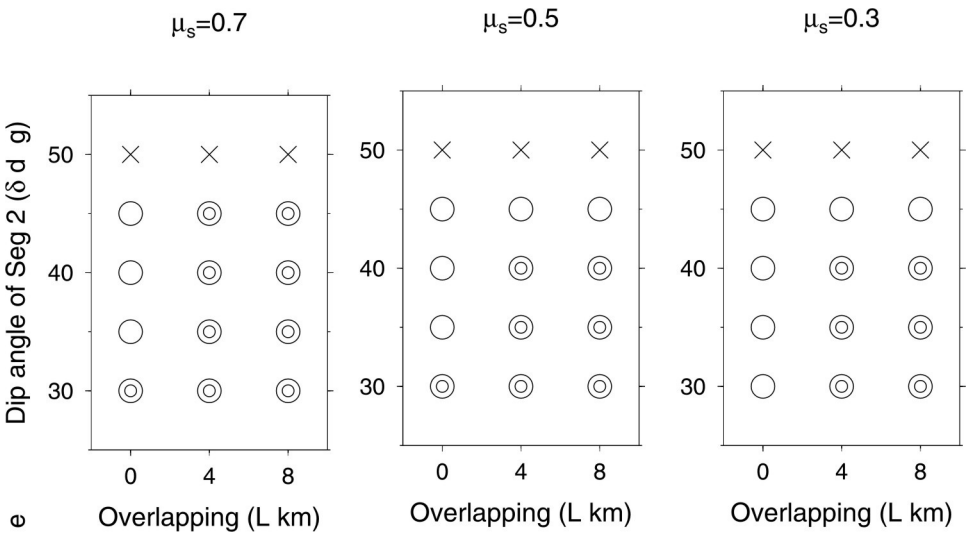
μs=0.7
μs=0.5
μs=0.3
Dip angle of Seg 2 (δ d g)
50
40
30
0
4
8
Overlapping (L km)

e

Figure 6.

1

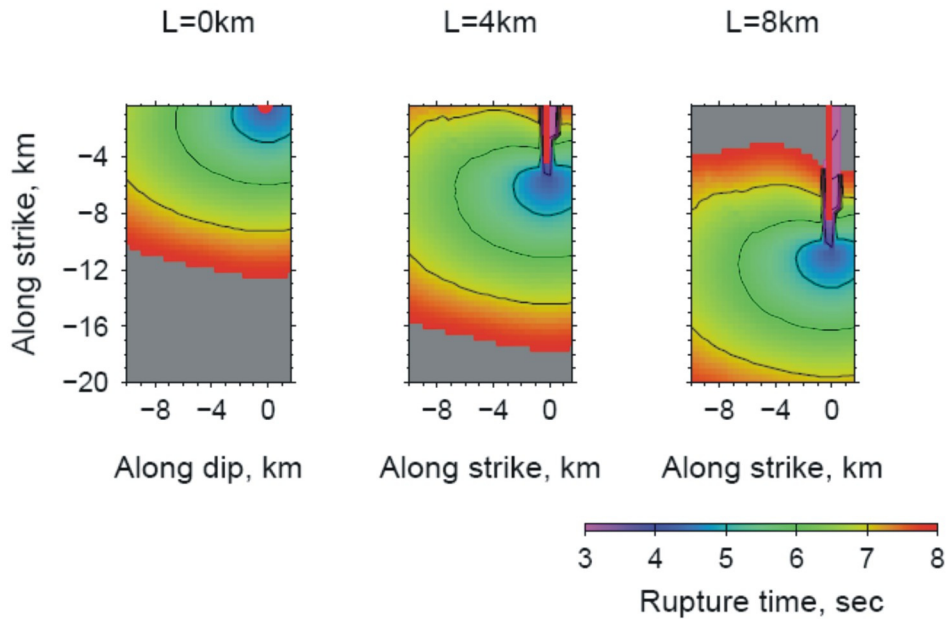
L=0km
L=4km
L=8km
Along strike, km
−4
−8
−12
−16
−20
−8 −4 0
Along dip, km
−8 −4 0
Along strike, km
−8 −4 0
Along strike, km
3 4 5 6 7 8
Rupture time, sec

2

3 Figure 7.